Optimizing Arrays of Randomly Placed Wireless Transmitters for Receivers Located Within the Array Volume

William F. Young, *Member, IEEE*, Edward F. Kuester, *Fellow, IEEE*, and Christopher L. Holloway, *Senior Member, IEEE*

***Abstract*—We investigate the potential of using arbitrarily placed wireless transceivers to increase the probability of maintaining a communication link in an electrically harsh environment. Specifically, we adapt a well-known matrix-based array optimization technique to the case when the transmitting elements exist in a complex environment and the receiver is not in the far-field of the array. Study of array performance in a non-ideal setting represents an important step in determining the feasibility of using this optimization technique for *ad hoc* wireless arrays within a building. Measures of array performance consist of median values for the directivity or gain, the total power at the receiver location, and the power per transmitter. The simulation results include array performance in the presence of a lossy dielectric corner to study the effects of building floors and walls. Our results show the median of the optimized directivity or gain for the frequencies of interest with simple boundaries is within 3 dB of that for the optimized configuration in free space.**

***Index Terms*—*Ad hoc* array, arbitrary array optimization, emergency responder communications, random array.**

I. Introduction

WIRELESS communication represents a key supporting technology to the success of an emergency responder. Unfortunately, a typical emergency response scenario involves communication into building structures, which can severely interfere with or completely block radio-frequency (RF) communcications. Measured results of RF attenuation behavior encountered by emergency responders in large buildings has been given in [1]–[4], and indicate large attenuation and high variability of signal strength. One potential method of improving the RF channel within a building utilizes the intelligent control of the electromagnetic radiation from wireless devices quickly placed at random locations in the building during entry by the emergency responder. These devices would perform as antenna array elements to improve communication capability for emergency responders both within the structure and with external personnel. In this paper, we present our analysis and simulation results for optimized arrays of arbitrarily located radio transceivers aimed at improving the design of wireless communication systems used in current and future emergency response scenarios.

Array directivity or gain optimization techniques based on a generalized matrix eigenvalue problem are well covered in past literature, [5]–[9], with [10]–[12] focused on constrained optimization, and a more recent publication [13] providing a detailed mathematical development on the topic of optimized electromagnetic radiation. In addition, probabilistic approaches to antenna array analysis and synthesis are discussed in [14]–[17]. However, to the best of our knowledge, the application of array optimization concepts to arbitrarily located wireless transmitters with the receiver located within or near the array represents a new area of investigation.

Our application of the optimization technique to arbitrary transmitter locations differs from the typical approach to antenna array optimization in three key ways. First, the receiver location, or the desired point of optimum radiation is now within or near the volume of the array, which requires the use of a slightly modified expression for "gain" or "directivity" as a performance index. Second, we examine the statistical behavior of the optimized performance, i.e., median gain, by optimizing a large number of sets of random transmitter and receiver locations. Third, the effects of some simple boundary surfaces are included through the use of Green's functions and first order impedance boundary conditions, where the boundaries are chosen as representative of the complex real-world environment. This last item, discussed in [18], pertains to work on arrays in arbitrary environments. Fig. 1 depicts four transmitters and a receiver within a bounded volume, and illustrates a general configuration for the problem.

We apply three measures of performance, i.e., directivity, total power at the receiver, and power per transmitter, to the array configuration, and compare the optimized results to self-phased arrays. Self-phased or co-phased arrays, discussed in [19]–[21], use phase conjugation of a pilot signal from the receiver to ensure that contributions from the transmitters arrive in-phase at the receiver. The optimized arrays are also co-phased with respect to the receiver location, but include transmitter amplitude control for overall system power efficiency, i.e., efficient use of the total power if all the available transmitters are utilized. Results from the three measures of performance suggest a fairly straightforward field-implementation.

Manuscript received April 3, 2006; revised December 5, 2006. This work was supported by Sandia National Laboratories and the National Institute of Standards and Technology.

W. F. Young is with the National Institute of Standards and Technology, Boulder, CO 80305-3328 USA on leave from Sandia National Laboratories, Albuquerque, NM 87185-0672 USA.

E. F. Kuester is with the Department of Electrical and Computer Engineering at the University of Colorado Boulder, CO 80309-0425 USA

C. L. Holloway is with the National Institute of Standards and Technology, Boulder, CO 80305-3328 USA.

Color versions of one or more of the figures in this paper are available online at http://ieeexplore.ieee.org.

Digital Object Identifier 10.1109/TAP.2007.891555

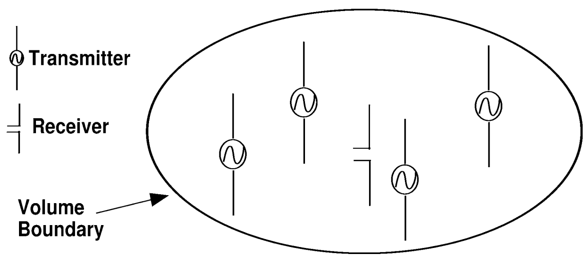

Fig. 1. General transmitter/receiver configuration.

While our proposed topology of wireless devices resembles an *ad hoc* network, our focus is not on *ad hoc* networks or protocols. We are studying the possibility of controlling the electromagnetic radiation of the wireless devices in aggregate so as to form an antenna array. This differs from the typical power control of a single device, which is used simply to control its radius of coverage, or to increase the battery life by limiting usage. A complete system using our approach will require various supporting protocols; however, we focus here on the electromagnetic behavior of the system.

The remainder of the paper proceeds as follows. Section II covers the supporting theory and simply boundary configurations, Section III includes the measures of performance, a simulation process description, and corresponding results, Section IV outlines an implementation approach, and finally, Section V contains the overall conclusions drawn in this research.

II. Theory

A. Approximate Green's Functions

The optimization process utilizes Green's functions for the volume of interest subject to some simple boundary conditions. Due to length considerations, here we only present the cases of 1) free space and 2) a corner reflector. This section details the Green's function development with the transmitters and receivers located in free space near a lossy dielectric corner as illustrated in Fig. 2. More details on the theory and additional simple boundary configurations are contained in [22] and [23], e.g., locating the array between perfect electric conducting (PEC) walls to investigate behavior in resonant or near resonant conditions. Note, while investigating the error introduced by each particular approximation in the analysis process would be an interesting endeavor, such activity would distract from the central theme of this work.

1) Free Space: Free space represents the simplest boundary condition, but allows comparisons to previous array optimization work in Section III. The mathematical representation follows as a limiting case of the corner reflector discussed next, with all Γ values set to zero.

2) Concrete and Soil Corner: A Hertzian dipole antenna represents the transmitters and receivers, and allows the investigation to focus on general array behavior rather than the effects of

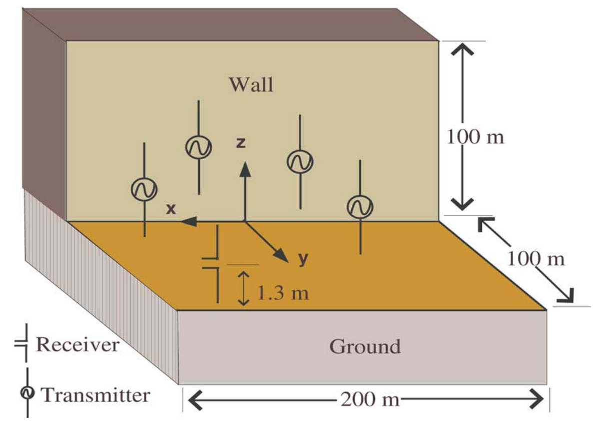

Fig. 2. Corner configuration. Uniformly random distributions over intervals in Table II, unless specified as a constant; minimum of 1.75 m between transmitters.

a specific antenna type. The nth Hertzian dipole source, i.e., the nth transmitter is defined as

$$\vec{J}_n = -\hat{z}\frac{a_n \delta(\vec{r}-\vec{r}_n)}{j\omega\mu_o} \tag{1}$$

where ω is the angular frequency, μ_o is the permeability of free space, a_n is the complex scaled current, and $\delta(\cdot)$ is the impulse or Dirac delta function. The two distance vectors $\vec{r}$ and $\vec{r}_n$, represent the observation and source points, respectively.

In order to reduce the numerical cost in computing the Green's functions for the boundaries under consideration, we make use of image theory and, in some configurations, approximate boundary conditions. Image theory requires locating an image of the source with a weight Γ, such that the replaced boundary condition is satisfied as closely as possible. For example, if the transmitter is located in free space near a dielectric corner as shown in Fig. 2, the approximate vector Green's function for $y > 0$, $z > 0$ takes the following form:

$$\vec{G}^z(\vec{r},\vec{r}_n) = \hat{z}G(\vec{r},\vec{r}_n) + \frac{1}{k^2}\nabla\nabla\cdot\hat{z}G(\vec{r},\vec{r}_n) \tag{2}$$

where $G(\vec{r},\vec{r}_n)$ is a solution to the scalar wave equation

$$(\nabla^2 + k^2)G(\vec{r},\vec{r}_n) = -\delta(\vec{r}-\vec{r}_n). \tag{3}$$

The scalar Green's function in (3) takes the form

$$\begin{aligned} G(\vec{r},\vec{r}_n) = {} & \frac{e^{-jk|\vec{r}-\vec{r}_n|}}{4\pi|\vec{r}-\vec{r}_n|} + \Gamma_1\frac{e^{-jk\left|\vec{r}-\vec{r}_n^{(1)}\right|}}{4\pi\left|\vec{r}-\vec{r}_n^{(1)}\right|} \\ & + \Gamma_2\frac{e^{-jk\left|\vec{r}-\vec{r}_n^{(2)}\right|}}{4\pi\left|\vec{r}-\vec{r}_n^{(2)}\right|} + \Gamma_3\frac{e^{-jk\left|\vec{r}-\vec{r}_n^{(3)}\right|}}{4\pi\left|\vec{r}-\vec{r}_n^{(3)}\right|} \end{aligned} \tag{4}$$

where

$$\vec{r}_n = (x_n, y_n, z_n), \quad \vec{r}_n^{(1)} = (x_n, y_n, -z_n)$$
$$\vec{r}_n^{(2)} = (x_n, -y_n, z_n), \quad \vec{r}_n^{(3)} = (x_n, -y_n, -z_n)$$

and $k = 2\pi/\lambda$. Note that the superscript on $\vec{G}^z$ in (2) refers to the direction or orientation of the source.

The Silver-Müller radiation conditions are appropriate for the quarter-spherical surface at infinity, and are given as [13, pp. 60–62]

$$\lim_{r\to\infty} r\left[\hat{a}_r \times \vec{H} + \frac{1}{\eta_o}\vec{E}\right] = 0$$
$$\lim_{r\to\infty} r\left[\hat{a}_r \times \vec{E} - \eta_o\vec{H}\right] = 0 \tag{5}$$

where $\eta_o = \sqrt{\mu_o/\epsilon_o}$ is the wave impedance of free space. We use a first order impedance boundary condition to approximate the dielectric wall and ground boundaries. This approximate boundary condition takes the form [25]

$$\hat{n} \times \vec{E} = \eta\hat{n} \times (\hat{n} \times \vec{H}) \tag{6}$$

where $\hat{n}$ is the outward normal to the surface, μ is the permeability, ϵ is the permittivity of the material, and $\eta = \sqrt{\mu/\epsilon}$ is the impedance of the material. (6) should be accurate provided the magnitude of the complex ϵ of the material creating the boundary is large enough. The electric field in the region ($y > 0$, $z > 0$) due to the Hertzian dipole source at $\vec{r}_n$ is equal to the Green's function plus the surface integral

$$\oint_S \left(\vec{G}^z(\vec{r}\,', \vec{r}_n) \times \nabla' \times \vec{E}(\vec{r}\,') - \vec{E}(\vec{r}\,') \times \nabla' \times \vec{G}^z(\vec{r}\,', \vec{r}_n)\right) \cdot \hat{n} ds'. \tag{7}$$

An exact solution for the electric field would require this surface integral vanish, so we choose the weights Γ_i to minimize the residual surface integral. The Green's function given by (2) satisfies the radiation boundary condition (5), so the quarter-spherical surface at $r = \infty$ provides no contribution to the integral. The remaining surface of integration consists of the ground and wall surfaces. Using the first order impedance boundary condition (6), the relation $\nabla \times \vec{E} = -j\omega\mu_o\vec{H}$, and some vector manipulations, the following residual surface integral arises.

$$\int_S \left[\left(\hat{n} \times \vec{H}(\vec{r}\,')\right) \cdot \left(j\omega\mu_o\vec{G}^z(\vec{r}\,', \vec{r}_n) - \left\{\left[\nabla' \times \vec{G}^z(\vec{r}\,', \vec{r}_n)\right] \times \hat{n}\eta\right\}\right)\right] ds' \tag{8}$$

where η is computed from the material parameters, and the half-planes $(x, y \geq 0, z = 0)$ and $(x, y = 0, z \geq 0)$ are the surface of integration.

We work with the second of the dot product terms in the integrand of (8) to minimize the residual integral in the following manner. We integrate with respect to s' to remove the receiver location dependency, and then determine the maximum value of the magnitude squared with respect to the Γs. Interchanging the partial differentiations with the integration, letting $\eta = \eta_{\mathrm{soil}}$ with $\hat{n} = \hat{z}$ on the $z = 0$ surface, and $\eta = \eta_{\mathrm{concrete}}$ with $\hat{n} = \hat{y}$ on the $y = 0$ surface, leads to the following three equations that are solved simultaneously:

$$\int_S \left[\frac{\partial}{\partial\Gamma_i^*}\left|(j\omega\mu_o\vec{G}^{z,\Gamma} - \left\{[\nabla \times \vec{G}^{z,\Gamma}] \times \eta\vec{n}\right\}\right|^2\right] ds' = 0 \tag{9}$$

for $i = 1, 2, 3$, where

$$\vec{G}^{z,\Gamma} = \vec{G}^z\left(\Gamma_1, \Gamma_2, \Gamma_3, \vec{r}\,', \vec{r}_n, \vec{r}_n^{\,(1)}, \vec{r}_n^{\,(2)}, \vec{r}_n^{\,(3)}\right) \tag{10}$$

is the vector Green's function (2), and explicitly shows the dependence on the Γ values and the source image terms. The $*$ denotes complex conjugation.

The partial derivatives are expressed in closed form, while the integrations are performed numerically in the simulations (the numerical integration limits are shown in Fig. 2). We should emphasize that the impedance boundary condition is not expected to be very accurate for higher frequencies or low permittivities, but since our goal here is to assess the order of magnitude of environmental effects, this model is adequate for our purposes. The special case free space is obtained by simply taking all Γ values to be zero. For the limiting case of a PEC corner, infinite over the half-planes $(x, y \geq 0, z = 0)$ and $(x, y = 0, z \geq 0)$, with $\hat{z}$-oriented transmitters, $\Gamma_{1,2,3}$ become $+1$, -1, and -1, respectively.

B. Modified Directivity

Directivity or gain is one of the performance indices or measures, but here we are not assuming that the receiver lies in the far field of the array. Rather, the receiver is actually within or near the volume of the array of transmitters, and thus we require modification of the standard directivity equation [26]. To this end, we define a performance index p in the following manner:

$$p = \frac{4\pi \times \text{radiation intensity}}{\text{system input power}} = \frac{4\pi\frac{R_{ave}^2\left|\vec{u}_p \cdot \vec{E}(\vec{r})\right|^2}{2\eta_o}}{-\frac{1}{2}\mathrm{Re}\int_V \vec{E}(\vec{r}) \cdot \vec{J}^*(\vec{r})dv}. \tag{11}$$

In the numerator, $\vec{u}_p$ is the receive antenna polarization unit vector, $\vec{E}(\vec{r})$ is the total electric field at location $\vec{r}$, R_{ave} is the average distance between the transmitters and receiver, calculated by

$$R_{ave} = \sqrt{1\Big/\left(N\sum_{n=1}^{N} 1/R_n^2\right)} \tag{12}$$

where R_n^2 is the squared distance between the nth transmitter and the receiver, and N is the total number of transmitters. In this work we assume $\vec{u}_p = \hat{z}$. The quantity R_{ave} represents a change from the typical far-field description of radiation intensity, where all the elements are approximately the same distance from the observation point. However, we want to account for individual magnitude differences due to transmitter locations in our performance index. Thus, (12) averages out the $1/R^2$ magnitude behavior of the received power when the receiver is near the array.

In the denominator, $\vec{J}^*(\vec{r})$ is the conjugate of the current source at $\vec{r}$. The volume integral includes all the source locations.

C. Optimization of the Modified Directivity Equation

The modified directivity (11) measures the effectiveness in utilizing transmitters as array elements versus an isotropic source for radiating electromagnetic energy. Increasing the directivity or gain over an isotropic source requires optimizing the a_n or scaled currents in (1) for each individual transmitter, with the receiver at a specified location within the array volume.

We optimize (11) with respect to the transmitter currents using the following approach.

Since the transmitters are discrete radiators, (11) may be rewritten in a form consistent with the matrix optimization procedure as follows. A single transmitter represented by (1) creates an electric field

$$\vec{E}_n(\vec{r}) = a_n \vec{G}^z(\vec{r}, \vec{r}_n) \tag{13}$$

which is the electric field at location $\vec{r}$, due to a transmitter at location $\vec{r}_n$. The total electric field $\vec{E}(\vec{r})$ is the sum of the fields created by each transmitter. That is

$$\vec{E}(\vec{r}) = \sum_{n=1}^{N} \vec{E}_n(\vec{r}) = \sum_{n=1}^{N} \vec{E}(\vec{r}, \vec{r}_n) \tag{14}$$

where $\vec{r}_n$ is the location of the nth transmitter and N is the total number of transmitters. Then, the magnitude squared portion of the numerator in (11) can also be written as a double sum. Specifically, the magnitude squared of the received electric field in (11) is written as

$$\left|\vec{u}_p \cdot \vec{E}(\vec{r})\right|^2 = \sum_{m=1}^{N} \sum_{n=1}^{N} \left[\hat{z} \cdot \vec{E}_m^*(\vec{r})\right] \cdot \left[\hat{z} \cdot \vec{E}_n(\vec{r})\right]. \tag{15}$$

Since the receiver is polarized along $\hat{z}$, we need only the z-component of the electric field at the receiver. Let

$$\nu_n = \sqrt{4\pi} \frac{R_{ave}}{\sqrt{2\eta_o}} G_z^z(\vec{r}, \vec{r}_n), \quad \text{for } n = 1, 2, \dots N \tag{16}$$

where ν_n is the nth element of the column vector $\vec{\nu}$, and $G_z^z(\vec{r}, \vec{r}_n)$ is the z-component of (2). Then the numerator in (11) can be written as

$$4\pi \frac{R_{ave}^2 \left|\vec{E}(\vec{r})\right|^2}{2\eta_o} = \sum_{m=1}^{N} \sum_{n=1}^{N} a_m^* \nu_m^* \nu_n a_n. \tag{17}$$

In examining the denominator of (11), the input power involves the dot product with a z-directed impulse function

$$P_{\text{in}} = -\frac{1}{2} \text{Re} \int_V \sum_{n=1}^{N} \vec{E}(\vec{r}, \vec{r}_n) \cdot \left(\hat{z} \frac{a_m^* \delta(\vec{r} - \vec{r}_m)}{j\omega\mu_o}\right) dv. \tag{18}$$

The dot product reduces the contribution from the electric field to only the z-component, and the impulse function converts the volume integral to a summation over the indexed sources. Substituting in the Green's function form for the electric field, the total input power P_{in}, due to the N transmitters, takes the following form:

$$P_{\text{in}} = \frac{1}{2} \text{Re} \left[\frac{j}{\omega\mu_o} \sum_{n=1}^{N} \sum_{m=1}^{N} a_m^* a_n G_z(\vec{r}_m, \vec{r}_n)\right] \tag{19}$$

where $a_n G_z(\vec{r}_m, \vec{r}_n)$ is the z-component of the electric field due to the nth element at the location of the mth element. (To avoid the difficulty with the singularity in the imaginary part of the Green's function when $r_m = r_n$, we can assume a uniform current distribution on a small volume, perform the integration, take the real part of the result, and then let the size of the small volume approach zero. This is analogous to the approach in [8, pp. 199–200], with details specific to this application covered in [22, pp. 146–154]).

Now we can re-write (11) as

$$p(\vec{a}) = \frac{\sum_{m=1}^{N} \sum_{n=1}^{N} a_m^* \alpha_{mn} a_n}{\sum_{m=1}^{N} \sum_{n=1}^{N} a_m^* \beta_{mn} a_n} \tag{20}$$

where

$$\alpha_{mn} = \nu_m^* \nu_n \tag{21}$$

and

$$\beta_{mn} = \frac{1}{2} \text{Re} \left[\frac{j}{\omega\mu_o} G_z(\vec{r}_m, \vec{r}_n)\right]. \tag{22}$$

As discussed in Section I, many papers have covered the matrix optimization technique used here. We first present the important mathematical constructs which follow closely the work in [9], and then apply the technique to our specific performance index. We rewrite the performance index as

$$p(\vec{a}) = \frac{(\vec{a}^*)^\dagger \bar{A} \vec{a}}{(\vec{a}^*)^\dagger \bar{B} \vec{a}} \tag{23}$$

where

$$(\vec{a}^*)^\dagger = [a_1^*, a_2^*, \dots, a_N^*]$$

and we have defined the matrices

$$\bar{A} = [\alpha_{mn}] = \vec{\nu}^* \vec{\nu}^\dagger \text{ and } \bar{B} = [\beta_{mn}]$$

where † means the transpose of a vector. From matrix theory, if both $\bar{A}$ and $\bar{B}$ are $N \times N$ Hermitian matrices, where $\bar{A}$ is positive semi-definite, and $\bar{B}$ is positive definite, then

1) the eigenvalues of the generalized eigenvalue equation are real and positive

$$det(\bar{A} - \lambda \bar{B}) = 0 \tag{24}$$

where

$$\lambda_1 \geq \lambda_2 \geq \cdots \geq \lambda_N \in \Re.$$

2) λ_1 and λ_N bound $p(\vec{a})$,

$$\lambda_1 \geq p(\vec{a}) \geq \lambda_N \tag{25}$$

and the left equality in (25) occurs when $\vec{a}$ satisfies

$$\bar{A}\vec{a} = \lambda_1 \bar{B} \vec{a}. \tag{26}$$

In addition, the following optimization applies. Because $\bar{A}$ has the form $\vec{\nu}^* \vec{\nu}^\dagger$, there is only one nonzero root of (24), which corresponds to the optimized directivity

$$p_{opt} = \lambda_1 = \vec{\nu}^\dagger \bar{B}^{-1} \vec{\nu}^* > 0 \tag{27}$$

with the corresponding current eigenvector

$$\vec{a}_1 = \bar{B}^{-1} \vec{\nu}^*. \tag{28}$$

The optimization problem now reduces to solving for λ_1 and $\vec{a}_1$, which are the maximum directivity and optimized transmitter currents, respectively, for our specific performance index. For each scenario investigated, we derive ν_n and β_{mn} for simple boundary conditions, and then compute the maximum directivity or gain defined by (27).

Note that if the transmitters are all $\hat{z}$-directed, but the receiver is oriented at an angle θ from the z-axis, the $\hat{z}$ component is scaled by $\cos\theta$ in (16) and $\hat{x}$ and $\hat{y}$-components multiplied by $\sin\theta$ will be added. Since the sources are $\hat{z}$-directed, the decrease in gain basically follows a $\cos^2\theta$ dependency, due to small $\hat{x}$ and $\hat{y}$-directed field contributions to the total electric field for the boundary configurations of interest. This does not represent optimizing for arbitrary transmitter orientations as discussed in [27], but rather, allows an arbitrary receiver orientation *after* the optimization procedure.

This theoretical representation allows investigation into several different performance indices. Besides the modified directivity performance index, the total power at the receiver location and the power per transmitter performance measures are easily calculated using the optimized currents (28), as demonstrated in the next section.

III. Simulation

A. Measures of Performance

The three measures of performance are 1) modified directivity (27); 2) total power at the receiver location; and 3) power per transmitter at the receiver location. Actual received power depends on the specific receiver, but to capture individual transmitter effects, we utilize the following expression for normalized power at the receiver location:

$$P_i = \left|\vec{E}_i(\vec{r})\right|^2, \quad i = 1, 2, \ldots, N. \tag{29}$$

Recall that (13) allows explicit use of the transmitter currents in calculating $\vec{E}(\vec{r})$. Total normalized power P_{tot} is calculated by taking the ordered cumulative sum of the normalized power due to the M strongest transmitters, up to the total number of active transmitters, N. The describing equation is

$$P_{\text{tot}} = \left|\sum_{i=1}^{M} \vec{E}_i(\vec{r})\right|^2, \quad |\vec{E}_1| \geq |\vec{E}_2| \cdots \geq |\vec{E}_M|, \ M \leq N \tag{30}$$

where $\vec{E}_i$ is the electric field at the receiver location due to the ith transmitter. Power per transmitter is calculated by taking the magnitude squared of the ordered cumulative sum of the electric field due to the M strongest transmitters and dividing by the number of total number transmitters included in the sum

$$P_{\text{transmitter}} = \frac{\left|\sum_{i=1}^{M} \vec{E}_i(\vec{r})\right|^2}{M}, \quad P_1 \geq P_2 \ldots \geq P_M, \ M \leq N. \tag{31}$$

For all three performance measures, transmitter currents are either optimized currents (28) or unity amplitude, co-phased with respect to the receiver location, i.e., the electric field at the receiver location is in-phase for all the transmitter contributions. Note that the optimized currents are co-phased with respect to the receiver location, but are not of uniform amplitude. The electric fields due to co-phased currents are described by

$$\vec{E}_n(\vec{r}) = \phi_n \vec{G}^z(\vec{r}, \vec{r}_n) \tag{32}$$

where

$$\phi_n = \frac{a_n}{|a_n|} \tag{33}$$

and a_n is the nth element of (28). When computing the total power and power per transmitter, the optimized currents are normalized so that the largest individual current magnitude is unity.

B. Simulation Process Description

The simulation process consists of generating statistics for random array configurations with the simple boundary conditions discussed in Section II, at frequencies of 100 MHz, 1 GHz, and 5 GHz. Although we could have examined other configurations, the additional complexity would not necessarily improve the accuracy in modeling the real environment or our understanding of the array behavior. The steps in the simulation process are as follows.

1) Randomly locate 2–16 transmitters.
2) Generate 40 random receiver locations.
3) Compute optimized currents based on modified directivity performance index and co-phased transmitter currents for 40 receiver locations, subject to the boundary conditions and transmitter/receiver locations.
4) Collect median values for
   - modified directivity;
   - total power;
   - power per transmitter.
5) Perform steps 1 through 4 for two hundred trials.
6) Collect overall median values for
   - modified directivity;
   - total power;
   - power per transmitter.

Table II lists the location distribution intervals for the transmitters and receivers. A receiver height fixed at 1.3 m models the height of the receiver antenna on the emergency responder, and a minimum spacing of 1.75 m between transmitters corresponds to the transmitters as placed by emergency responders as they move through the building. Locating transmitters in a volume below the receivers models the anticipated relative positions be-

TABLE I
MATERIAL PROPERTIES FOR CONCRETE AND SOIL [24]

Frequency	Wall $\tan\delta_\epsilon$	Wall ϵ_r	Ground $\tan\delta_\epsilon$	Ground ϵ_r
100 MHz	0.0015	2.43	0.251	20
1 GHz	0.0010	2.43	0.056	20
5 GHz	0.00078	2.43	0.076	20
$\tan\delta_\epsilon$ = loss tangent; ϵ_r = relative permittivity				

TABLE II
TRANSMITTER AND RECEIVER LOCATION INTERVALS

	x	y	z
Transmitter	(-10 m, 10 m)	(0 m, 20 m)	(0.4 m, 0.75 m)
Receiver	(-10 m, 10 m)	(0 m, 20 m)	1.3 m

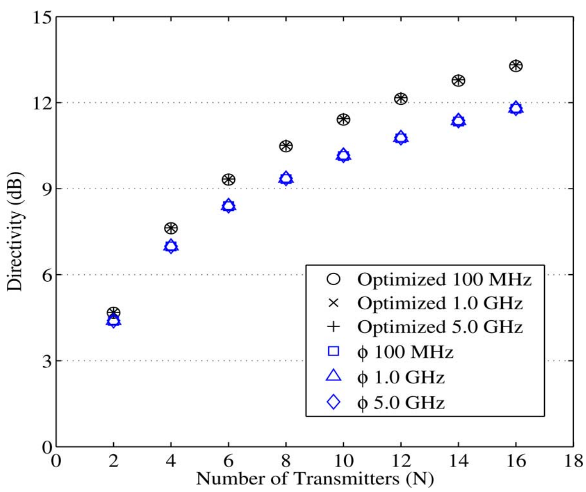

Fig. 3. Free space simulation results for transmitter and receiver locations over intervals in Table II. "Optimized" and "ϕ" represent optimized transmitter currents in (28) and co-phased, unity amplitude transmitter currents in (33), respectively.

tween transmitters and receivers in a field-implementation. The same locations are used for all the boundary scenarios to allow direct comparisons between different boundary results.

C. Free Space

Free space represents the first scenario, where all $\Gamma_i = 0$ in (2). The free space configuration allows comparison to some deterministic linear array results based on the same optimization technique, but using the standard definition of directivity, with the receiver in the far field of the array.

The simulation results for free space are shown in Fig. 3. As expected, for all number of transmitters, the median of the optimized directivity exceeds the co-phased results. The median results for our random arrays using the modified directivity equation are approximately 10.5 and 11.5 dB for eight and ten transmitters, respectively, for all three frequencies. All of these results compare reasonably well to results for linear arrays in the literature listed in Table III, particularly within the context of this analysis as discussed in Section I. When comparing the results, we need to keep in mind that the results in [9] and [8] are for the standard directivity with the observation point in the far-field of the array. Our results are for the modified directivity with the observation within the volume of the array. With confidence in the algorithms, the investigation now focuses on the total power at the receiver location and power per transmitter statistics.

TABLE III
OPTIMIZED LINEAR ARRAY RESULTS FROM LITERATURE

Number of Elements	Spacing	Array Type	Directivity
8 isotropic [8]	0.425λ	Endfire	13.4 dB
8 isotropic [8]	0.95λ	Endfire	10 dB
10 isotropic [9]	0.95λ	Endfire	11 dB
10 isotropic [9]	0.90λ	Broadside	12 dB
10 isotropic [9]	1.05λ	Broadside	9 dB

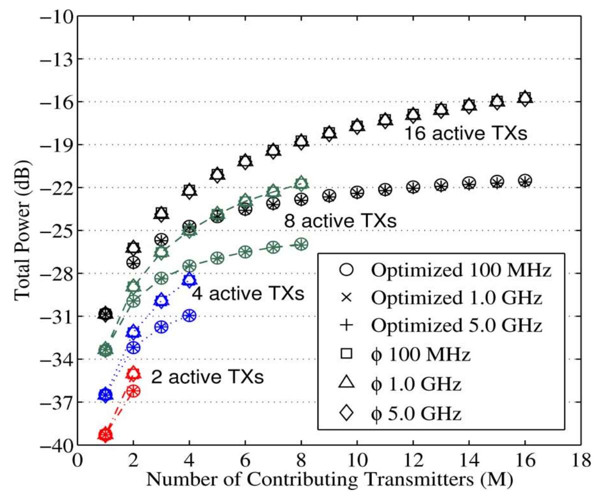

Fig. 4. Free space total power simulation results for transmitter (TX) and receiver locations over intervals in Table II. "Optimized" and "ϕ" represent transmitter currents (28) and (33), respectively. The maximum number of contributing transmitters on a particular curve equals the number of active transmitters generating that specific curve.

Fig. 4 shows the total power results for free space, with the four cases consisting of two, four, eight, and sixteen active transmitters. In the total power plots, the number of active transmitters refers to the number of transmitters turned on while computing (30). The number of contributing transmitters represents the ordered partial sums of the active transmitters, i.e., the value of M in (30). For example, in the case of four active transmitters, the partial sums consist of one, two, three, and four transmitters. Note that the co-phased approach sets all the transmitters at maximum power while the optimized method scales the individual transmitter power according to the performance index. Thus, the co-phased results indicate a greater total power at the receiver than the optimized results, but also require greater total system input power.

The spread of approximately 9 dB for a single contributing transmitter across the four cases of active transmitters reflects the difference in the average geometrical distance between the strongest transmitter and the receiver location. In other words, on average, the sixteen active transmitter case will have a transmitter much closer to the receiver location than if only two active transmitters are utilized. For the optimized case, the eight and sixteen number of active transmitter curves indicate that the

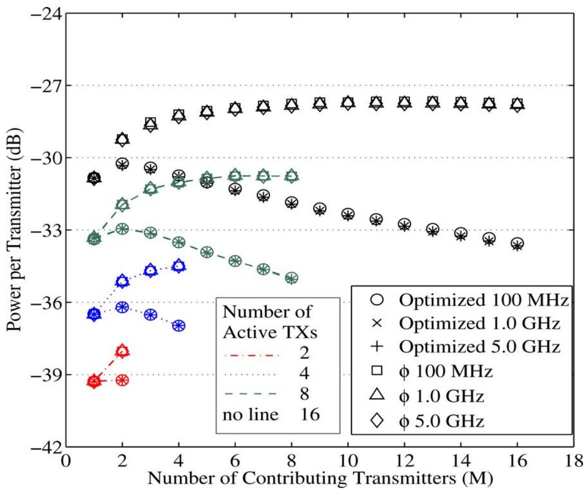

Fig. 5. Free space power per transmitter simulation results for transmitter and receiver locations over intervals in Table II. "Optimized" and "ϕ" represent (28) and (33) transmitter currents, respectively. The maximum number of contributing transmitters on a particular curve equals the number of active transmitters generating that specific curve.

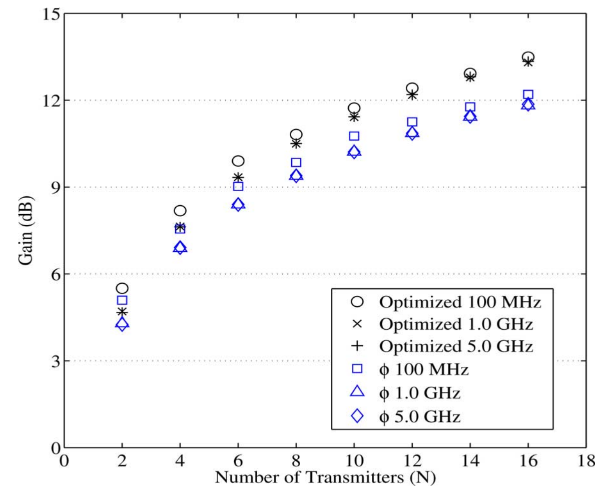

Fig. 6. Concrete and soil corner directivity simulation results for transmitter and receiver locations over intervals in Table II. "Optimized" and "ϕ" represent transmitter currents (28) and (33), respectively.

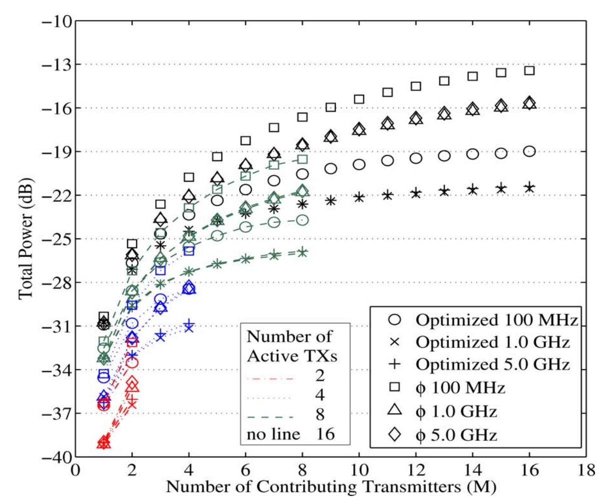

Fig. 7. Concrete and soil corner total power simulation results for transmitter and receiver locations over intervals in Table II. "Optimized" and "ϕ" represent transmitter currents (28) and (33), respectively. The maximum number of contributing transmitters on a particular curve equals the number of active transmitters generating that specific curve.

total power increases by less than 2 dB after four or six transmitters, respectively. While the co-phased case does not show as strong a limiting behavior, with sixteen active transmitters, a doubling of transmitters from two to four provides a 4.5 dB increase, but a doubling from eight to sixteen transmitters only increases the median power by 3 dB.

Fig. 5 shows the power per transmitter in free space. Two important observations are 1) the optimized array curves indicate a maximum at two transmitters for all cases, and 2) the co-phased results are within 1/2 dB of the maximum by four transmitters. The combination of these two results show that the two to four transmitters with the strongest signal at the receiver provide the greatest benefit in terms of the array gain. In free space, the strongest contributors would also be the geometrically closest. However, that will not necessarily be the case for other boundary configurations, such as the concrete and soil corner considered next.

D. Concrete and Soil Corner

Fig. 2 illustrates the concrete and soil corner configuration, where the image strengths, i.e., the Γ values, are found as described in Section II. Table II lists the transmitter and receiver locations, while Table I indicates the material properties for the three frequencies of interest. A complex permittivity incorporates loss in the boundary conditions, and thus implies that the directivity performance index represents array gain instead of array directivity. (Losses associated with individual transmitters and receivers are not included.)

The directivity results for a concrete and soil corner shown in Fig. 6 represent both the transmitters and receivers oriented in the $\hat{z}$ direction. The only significant difference from the free space results in Fig. 3 occurs at 100 MHz, where both the optimized and co-phased results indicate an increase over free space of approximately 1 dB. Both the 1 and 5 GHz cases are nearly the same as free space.

Fig. 7 depicts the total power for the concrete and soil corner. The 1 and 5 GHz cases are within 1 dB of the free space results shown in Fig. 4. However, both the optimized and co-phased results demonstrate approximately a 1.5 to 3 dB increase in total power at 100 MHz, depending on the number of active transmitters. The general trends of the curves match free space. For example, the gain increase associated with doubling from two to four transmitters is about 1.5 dB greater than when increasing from eight to sixteen transmitters of the co-phased results. Similarly for the optimized case, the eight and sixteen number of active transmitter curves indicate that the total power increases by less than 2 dB after four or eight transmitters, respectively.

The concrete and soil corner power per transmitter results are shown in Fig. 8. The 1 and 5 GHz curves are nearly identical to free space (see Fig. 5), but the 100 MHz curves indicate an increase between 1.5 to 3 dB over free space beyond six contributing transmitters for both the optimized and co-phased cases. In addition, the maximum shifts to three or four transmitters for the optimized case, and the point at which the co-phased

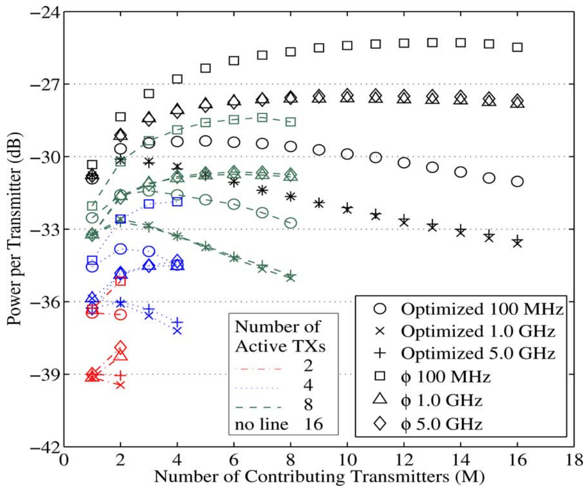

Fig. 8. Concrete and soil corner power per transmitter simulation results for transmitter and receiver locations over intervals in Table II. "Optimized" and "ϕ" represent transmitter currents (28) and (33), respectively. The maximum number of contributing transmitters on a particular curve equals the number of active transmitters generating that specific curve.

results are within 1/2 dB of the maximum occurs between four to seven transmitters. This suggests that a practical implementation will benefit from more than simply the two strongest contributing transmitters.

IV. Implementation

The three measures of performance point out some key behaviors that impact the field-implementation. First, diminishing returns in total power occur at approximately four transmitters for the optimized case and six to eight transmitters for the co-phased case. Secondly, the directivity results are not significantly different for the optimized and co-phased results. Thus, the following algorithm could be used to obtain results near the optimized.

1) Turn ON each transmitter individually, and determine the transmitter with the maximum contribution at the receiver.
2) Select the strongest contributing transmitter, and turn it ON with all the others OFF.
3) Select the next strongest transmitter determined in Step 1, and turn it ON.
   - Step the phase of this transmitter through 360°, and determine the phase when the peak power occurs at the receiver.
   - Set the phase of this transmitter to that corresponding to the maximum power at the receiver.
4) Repeat Step 3 for the remaining transmitters, until the desired number of contributing transmitters is reached.

This process will give the co-phased results for however many transmitters are included. If total system or radiated power is not a limitation, all the co-phased transmitters could be included in the process. However, if system power efficiency is important, say for example in a low power sensor network, then the optimized approach represents a more appropriate solution because it optimizes the power received at a particular location with respect to the total system input power. The optimization process reduces the power level of transmitters providing the weakest contribution at the receiver, which suggests only using the four or so strongest contributing transmitters. A reasonable approximation to the optimized solution is to use the algorithm above for a limited number of transmitters. To obtain the complete optimized result, the relative power level of each transmitter would also require adjustment.

V. Conclusion

We have investigated the performance of an array comprised of wireless transmitters in the presence of several simple boundary conditions that represent particular features of the complex real-world environment. In aggregate, the simulation results suggest that the combination of using wireless transceivers as an array with an optimization scheme can potentially improve the communication capability for emergency responders. These performance measures also demonstrate that the suggested implementation algorithm is applicable to systems where total input power is not a constraint, e.g., a temporary network for emergency responders, as well as to systems where power efficiency demands consideration, e.g., a lower power sensor network.

The combination of the three measures of performance suggests a straightforward algorithm for implementing such a system. Future work will focus on the testing the algorithm in a series of experiments in more complex environments, as well analyzing the sensitivity of such implementation. (Much of this work has been completed and will be published in the near future.) Dynamic updating will also be important, and [18] suggests that this is possible for wireless arrays; this will be the topic of further work.

Acknowledgment

The authors thank T. X. Brown, T. Mantueffel, and Z. Popović of the University of Colorado, and R. Wittmann of NIST, for their insightful suggestions.

References

[1] C. L. Holloway, G. Koepke, D. Camell, K. A. Remley, and S. Schima, "Shielding and attenuation properties of large buildings and structures," presented at the Proc. Eur. EMC Conf. Spain, Sep. 2006.
[2] C. L. Holloway, G. Koepke, D. Camell, K. Remley, D. Williams, S. Schima, S. Canales, and D. T. Tamura, "Propagation and detection of radio signals before, during and after the implosion of a thirteen story apartment building" NIST Tech. Note 1540,. Boulder, CO, May 2005 [Online]. Available: http://boulder.nist.gov/div818/81801/MetrologyForWirelessSys/index.html [Online]. Available: http://nvl.nist.gov/nist_pub_search.cfm?type=keyword)
[3] C. L. Holloway, G. Koepke, D. Camell, K. Remley, D. Williams, S. Schima, and S. Canales, "Propagation and detection of radio signals before, during and after the implosion of a large sports stadium (Veterans' Stadium in Philadelphia)" NIST Tech. Note 1541,. Boulder, CO, Oct. 2005.
[4] C. L. Holloway, G. Koepke, D. Camell, K. Remley, S. Schima, and R. T. Johnk, "Propagation and detection of radio signals before, during and after the implosion of a large convention center" NIST Tech. Note 1542,. Boulder, CO, Feb. 2006.
[5] J. L. Synge, "Directivity for scalar radiation," *Quarterly Appl. Math.*, vol. 24, no. 1, pp. 90–92, 1966.
[6] L. Susman and W. K. Kahn, "Measures of beam concentration for scalar radiation," *Radio Sci.*, vol. 5, no. 7, pp. 1091–1097, Jul. 1970.
[7] E. I. Krupitskii, "On the maximum directivity of antennas consisting of discrete radiators," *Sov. Phys. Dokl.*, vol. 7, pp. 257–259, 1962.

[8] R. F. Harrington, *Field Computation by Moment Methods*. New York: IEEE Press, 2000, ch. 10, (Reprint).

[9] D. K. Cheng and F. L. Tseng, "Gain optimization for arbitrary antenna arrays," *IEEE Trans. Antennas Propag.*, vol. 13, pp. 973–974, Nov. 1965.

[10] S. M. Sanzgiri and J. K. Butler, "Constrained optimization of the performance indices of arbitrary array elements," *IEEE Trans. Antennas Propag.*, vol. 19, no. 4, pp. 493–498, Jul. 1971.

[11] R. C. Voges and J. K. Butler, "Phase optimization of antenna array gain with constrained amplitude excitation," *IEEE Trans. Antennas Propag.*, vol. 20, no. 4, pp. 432–436, Jul. 1972.

[12] R. R. Kurth, "Optimization of array performance subject to multiple power pattern constraints," *IEEE Trans. Antennas Propag.*, vol. 22, no. 1, pp. 103–105, Jan. 1974.

[13] T. S. Angell and A. Kirsch, *Optimization Methods in Electromagnetic Radiation*. New York: Springer, 2004.

[14] Y. T. Lo, "A probabilistic approach to large aperiodic antenna arrays," in *Proc. Application Forum on Antenna Research*, Urbana, IL, Jan. 27–30, 1964, pp. 580–610.

[15] Y. S. Shifrin, *Statistical Antenna Theory*. Boulder, CO: The Golem Press, 1971.

[16] Y. T. Lo and S. W. Lee, Eds., *Antenna Handbook: Theory, Applications, and Design*. New York: Van Nostrand Reinhold, 1988, ch. 14.

[17] W. J. L. Queiroz and M. S. Alencar, "Project of antenna arrays with random parameters," in *Proc. Brazilian Microwave and Optoelectronics Society/Microwave Theory and Techniques Society, Int. Microwave and Optoelectronics Conf.*, Iguaza Falls, Brazil, Sep. 20–23, 2003, pp. 33–38.

[18] S. P. Morgan, "Interaction of adaptive antenna arrays in an arbitrary environment," *Bell Syst. Tech. J.*, vol. 44, pp. 23–47, 1965.

[19] M. I. Skolnik and D. D. King, "Self-phasing array antennas," *IEEE Trans. Antennas Propag.*, vol. 12, no. 2, pp. 142–149, Mar. 1964.

[20] L. D. DiDomenico and G. M. Rebeiz, "Digital communications using self-phased arrays," *IEEE Trans. Microw. Theory Tech.*, vol. 49, no. 4, pp. 677–684, Apr. 2004.

[21] S. Yen and T. Chu, "A retro-directive antenna array with phase conjugation circuit using subharmonically injection-locked self-oscillating mixer," *IEEE Trans. Antennas Propag.*, vol. 52, no. 1, pp. 154–164, Jan. 2004.

[22] W. F. Young, "Optimizing arrays of randomly placed wireless transmitters with receivers located in the array volume," Ph.D. dissertation, University of Colorado, Boulder, CO, to be published.

[23] W. F. Young, E. F. Kuester, and C. L. Holloway, Optimized arbitrary wireless device arrays for emergency response communications NIST Tech. Note 1538. Boulder, CO, Mar. 2005 [Online]. Available: http://boulder.nist.gov/div818/81801/MetrologyForWirelessSys/index.html [Online]. Available: http://nvl.nist.gov/nist_pub_search.cfm?type=keyword)

[24] A. R. Von Hippel, *Dielectric Materials and Applications*. New York: The Technology Press of MIT /Wiley, 1964, pp. 314–356.

[25] T. B. A. Senior and J. L. Volakis, *Approximate Boundary Conditions in Electromagnetics*. London, U.K.: IEE, 1995, ch. 2.

[26] C. A. Balanis, *Antenna Theory: Analysis and Design*, 2nd ed. New York: Wiley, 1989, p. 38, eqn.(2-12a).

[27] J. Sahalos, "On the optimum directivity of antenna consisting of arbitrarily oriented dipoles," *IEEE Trans. Antennas Propag.*, vol. 24, no. 3, pp. 322–327, May 1976.

[28] A. I. Uzkov, "An approach to the problem of optimum directive antenna design," *Dokl. Akad. Nauk. SSSR*, vol. 53, pp. 35–38, 1946.

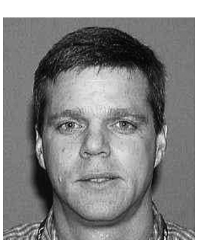

William F. Young (M'06) was born in Ponape, Micronesia, in 1966. He received the B.S. degree in electronic engineering technology from Central Washington University, Ellensburg, WA, in 1992, the M.S. degree in electrical engineering from Washington State University at Pullman, in 1998, and the Ph.D. degree from the University of Colorado at Boulder, in 2006.

Since 1998, he has worked for Sandia National Laboratories in Albuquerque, NM. His work at Sandia focused on the analysis and design of cyber security mechanisms for both wired and wireless communication systems used in the National Infrastructure and the Department of Defense. Currently, he is on leave from Sandia and is a Guest Researcher at the National Institute of Standards and Technology in Boulder, CO, and is working on improving wireless communication systems for emergency responders. His current research interests are in electromagnetic propagation for wireless systems, and the impacts of the wireless channel on overall communication network behavior.

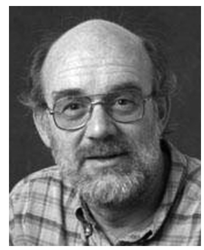

Edward F. Kuester (S'73–M'76–SM'95–F'98) received the B.S. degree from Michigan State University, East Lansing, in 1971, and the M.S. and Ph.D. degrees from the University of Colorado at Boulder, in 1974 and 1976, respectively, all in electrical engineering.

Since 1976, he has been with the Department of Electrical and Computer Engineering at the University of Colorado at Boulder, where he is currently a Professor. In 1979, he was a Summer Faculty Fellow at the Jet Propulsion Laboratory, Pasadena, CA. From 1981 to 1982, he was a Visiting Professor at the Technische Hogeschool, Delft, The Netherlands. In 1992 and 1993, he was an Invited Professor at the École Polytechnique Fédérale de Lausanne, Switzerland. He has held the position of Visiting Scientist at the National Institute of Standards and Technology (NIST), Boulder, CO in 2002, 2004, and 2006. His research interests include the modeling of electromagnetic phenomena of guiding and radiating structures, applied mathematics and applied physics. He is the coauthor of one book, author of chapters in two others, and has translated two books from Russian. He is co-holder of two U.S. patents, and author or coauthor of more than 60 papers in refereed technical journals.

Dr. Kuester is a member of the Society for Industrial and Applied Mathematics (SIAM) and Commissions B and D of the International Union of Radio Science (URSI).

Christopher L. Holloway (S'86–M'92–SM'04) was born in Chattanooga, TN, on March 26, 1962. He received the B.S. degree from the University of Tennessee at Chattanooga, in 1986 and the M.S. and Ph.D. degrees from the University of Colorado at Boulder, in 1988 and 1992, respectively, both in electrical engineering.

During 1992, he was a Research Scientist with Electro Magnetic Applications, Inc., in Lakewood, CO. His responsibilities included theoretical analysis and finite-difference time-domain modeling of various electromagnetic problems. From fall of 1992 to 1994, he was with the National Center for Atmospheric Research (NCAR) in Boulder, CO. While at NCAR his duties included wave propagation modeling, signal processing studies, and radar systems design. From 1994 to 2000, he was with the Institute for Telecommunication Sciences (ITS) at the U.S. Department of Commerce in Boulder, where he was involved in wave propagation studies. Since 2000, he has been with the National Institute of Standards and Technology (NIST), Boulder, where he works on electromagnetic theory. He is also on the Graduate Faculty at the University of Colorado at Boulder. His research interests include electromagnetic field theory, wave propagation, guided wave structures, remote sensing, numerical methods, and EMC/EMI issues.

Dr. Holloway is a member of Commission A of the International Union of Radio Science (URSI). He was awarded the 2006 Department of Commerce Bronze Medal for his work on radio-wave propagation, the 1999 Department of Commerce Silver Medal for his work in electromagnetic theory, and the 1998 Department of Commerce Bronze Medal for his work on printed circuit boards. He is an Associate Editor for the IEEE TRANSACTIONS ON ELECTROMAGNETIC COMPATIBILITY. He was the Chairman for the Technical Committee on Computational Electromagnetics (TC-9) of the IEEE Electromagnetic Compatibility Society from 2000 to 2005. He is currently serving as an IEEE Distinguished lecturer for the EMC Society.